Plasma effect on the phase matching of high harmonic generation

Hui Lu (芦 慧), Candong Liu (刘灿东), Shitong Zhao (赵诗童), and Peng Liu (刘 鹏)*

Shanghai Institute of Optics and Fine Mechanics, Chinese Academy of Sciences, Shanghai 201800, China

**Corresponding author: peng@siom.ac.cn*

Received May 31, 2010; accepted September 10, 2010; posted online January 1, 2011

By optimizing the phase matching condition of high harmonic generation (HHG) from a supersonic neon gas jet, the enhanced HHG in the region of 60−70 eV has been selected. Three-dimensional numerical calculation shows that plasma plays a significant role in the phase matching process of HHG in a supersonic gas jet with short medium length. Due to plasma formation, the harmonic emission decays as the laser intensity reaches over 3.5×10^{14} W/cm^2. The plasma induces the broadening and blue shift of the HHG spectra, which provides a method for fine-tuning the harmonic wavelength.

OCIS codes: 190.4160, 190.7110, 350.5400.
doi: 10.3788/COL201109.011901.

High harmonic generation (HHG) driven by ultrafast lasers provides a way to produce spatially and temporally coherent light radiation down to the extreme-ultraviolet and X-ray regions. This is increasingly used in applications such as atomic and molecular spectroscopy, plasma physics, and coherent imaging[1−3]. Conforming to the different application requirements, great efforts have been made either to increase the harmonic conversion efficiency, especially in the X-ray spectrum region through phase matching or quasi-phase matching methods[4,5], or to temporally confine the harmonic emission down to the attosecond timescale to generate an isolated attosecond laser pulse or a train of attosecond laser pulses[6−11].

A capillary setup is often used to increase the conversion efficiency of the harmonic emission. With long wavelength laser pre-excitation in the capillary, the generated phase-matched X-ray photon energy may be as high as 330 eV[5]. However, the capillary setup suffers from alignment difficulties and low laser damage thresholds. Moreover, it is very sensitive to the driving laser mode in the capillary so that it poses a strict requirement for the focusing stability of the driving laser pulses[12]. On the other hand, these problems are not encountered with a supersonic gas jet setup. A supersonic gas jet can support a short medium length (less than the Rayleigh length) laser beam, which makes the propagation effect on the harmonic generation due to laser beam geometry less significant. As a result, the gas jet setup is often applied in studies that require little or no influence of propagation, such as molecular orbital structure reconstruction from molecule HHG with sub-femtosecond resolution[13,14]. In these studies, the propagation has been neglected in the analysis for simplicity even though its influence is not well understood.

In this letter, we investigate the HHG phase matching process in a supersonic neon gas jet and obtain an enhanced HHG in the plateau region around harmonic order $q = 43$ (photon energy of 60−70 eV). As the driving laser intensity increases, the harmonic intensities are enhanced and then decreased. Moreover, the spectrum is broadened and blue shifted. The three-dimensional (3D) numerical model is established to show that the ionization-induced phase matching effect is responsible for the driving laser intensity dependence. The ionization results in not only the decreased macroscopic response of HHG but also a blue shift of the HHG spectra, which provides a method for fine-tuning the harmonic wavelength.

The experiments were performed using a commercial chirped-pulse-amplified (CPA) Ti:sapphire laser system with a repetition rate of 1 kHz, a central wavelength of 800 nm, a pulse duration of 50 fs, and a beam diameter of 12 mm at 90% peak intensity (Legend-USP-HE followed by a cryogenic multi-pass amplifier, Coherent Inc.). The output laser beam from the system was focused by a 300-mm focal length lens into the neon gas jet. Then, the generated harmonic emission was detected by a home-built flat-field X-ray spectrograph consisting of a gold-coated spherical mirror, a gold-coated cylindrical mirror, a Hamamatsu flat field grating, and a charge-coupled device (CCD) camera. To investigate HHG in the plateau region below 80 eV, an aluminum metal filter was applied before the spectrograph to separate the harmonics from the driving laser beam. In experiment, the confocal parameter of the laser beam was determined as 4 mm by measuring the laser beam size at a series of positions around the focus. The energy of the laser, with a maximum of 10 mJ/pulse, was varied using a half wave plate and a high contrast reflective polarizer. The laser pulse energy was calibrated as a function of the rotation angle of the half wave plate. The gas jet, with a diameter of 250 μm, had an effective interaction length of about 1.0 mm. The gas density in the jet had been tuned between 0 and 1.33×10^4 Pa by choosing different backing pressure between 0 and 5×10^5 Pa.

We measured the dependence of the harmonic intensity under a series of gas pressures. The high harmonic signal is only detectable under backing pressures above 2×10^5 Pa. As the backing pressure increases beyond 2×10^5 Pa, the high harmonic signal is constantly enhanced over the whole plateau spectrum explored here, indicating that dispersion-induced phase mismatching

may be neglected in the supersonic gas jet setup. This pressure-dependence trend agrees well with that in Ref. [15], except that in this case, a higher pressure, a shorter medium length, and a lower order spectrum region are investigated. Therefore, in the following experiment, considering the compression strength of the gas container, we set the backing pressure for the jet at 5×10^5 Pa to obtain the best output brilliance unless otherwise mentioned.

We then explored how the driving laser intensity affected the conversion efficiencies of the harmonics by scanning the driving laser intensities between 1×10^{14} and 1×10^{15} W/cm^2. Figure 1(a) shows the measured harmonic signal as a function of the driving laser intensity when the laser beam is focused 2 mm before the neon gas jet. At the 55−72 eV range, the harmonics have three noticeable features: 1) the harmonic signal reaches its maximum at around 3.9×10^{14} W/cm^2 intensity and then drops rapidly as the intensity increases further; 2) at driving laser intensities ranging from 3×10^{14} to 6×10^{14} W/cm^2, the harmonics are strong narrow spectral lines moving towards the blue band as the intensity rises; 3) for higher intensities, the harmonic spectrum broadens more towards the blue band and increases with the intensity, achieving $\Delta E \approx 0.15$ eV at 1×10^{15} W/cm^2. We attribute these features to the ionization-induced macroscopic effect, consistent with our simulations below. A similar intensity-dependent trend is also observed in Fig. 1(b) where the laser beam is focused 4 mm before the gas jet, except that the optimized driving laser intensity for the maximum harmonic emission is slightly lower than that in the former case. This difference may be attributed to the different phase matching conditions introduced by the different laser beam geometries. For the qth harmonic, the total phase mismatch can be described as

$$\Delta k_q = (k_q - qk_1) = \Delta k_{q,\mathrm{disp}} + \Delta k_{q,\mathrm{plasma}} + \Delta k_{q,\mathrm{foc}}, \quad (1)$$

where k_q and k_1 are the wave vectors of the qth harmonic field and the driving laser field, respectively, and $\Delta k_{q,\mathrm{disp}}$, $\Delta k_{q,\mathrm{plasma}}$, and $\Delta k_{q,\mathrm{foc}}$ are the wave vector mismatches for the qth harmonic due to atomic dispersion, plasma contribution, and geometric dispersion, respectively. For the gas jet setup, $\Delta k_{q,\mathrm{disp}}$ and $\Delta k_{q,\mathrm{foc}}$ are positive, whereas $\Delta k_{q,\mathrm{plasma}}$ is negative. To achieve full phase matching, the phase mismatches from $\Delta k_{q,\mathrm{disp}}$ and $\Delta k_{q,\mathrm{foc}}$ should be balance with the phase mismatch from $\Delta k_{q,\mathrm{plasma}}$. In the situation discussed above, $\Delta k_{q,\mathrm{foc}}$ for the gas jet positioned at $z = 2$ mm is larger than that at $z = 4$ mm, thus requiring a higher driving laser intensity to introduce a larger amount of $\Delta k_{q,\mathrm{plasma}}$ to equilibrate and achieve the best harmonic emission. However, as shown in Figs. 1(a) and (b), this optimized intensity difference (3.9×10^{14} and 3.5×10^{14} W/cm^2, respectively) is minimal, indicating that in supersonic gas jet, the laser beam geometry-induced phase mismatch may be neglected.

To study the plasma effects on the phase matching process of HHG, we performed 3D numerical simulations using the theoretical model proposed in Ref. [16], which is based on the numerical solution of Maxwell's equations in the frequency domain. The source term in Maxwell's equations for the harmonics is the microcosmic single-

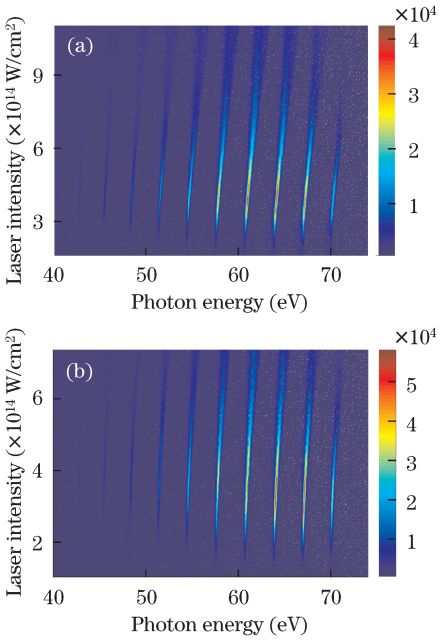

Fig. 1. Measured harmonic spectra as a function of the driving laser intensity when the supersonic neon gas jet is positioned at (a) $z = 2$ mm and (b) $z = 4$ mm.

atom response calculated using a strong-field approximation (SFA) model[17]. The propagation equations are described as

$$\nabla_\perp^2 \widetilde{E}_\mathrm{l}(r,z,\omega) - \frac{2\mathrm{i}\omega}{c}\frac{\partial \widetilde{E}_\mathrm{l}(r,z,\omega)}{\partial z} = \widetilde{G}_\mathrm{l}(r,z,\omega) \quad (2)$$

and

$$\nabla_\perp^2 \widetilde{E}_\mathrm{h}(r,z,\omega) - \frac{2\mathrm{i}\omega}{c}\frac{\partial^2 \widetilde{E}_\mathrm{h}(r,z,\omega)}{\partial z'} = -\omega^2 \mu_0 \widetilde{P}_\mathrm{nl}(r,z,\omega) \quad (3)$$

for the driving laser and for the harmonics, respectively. In Eq. (2), c is the light velocity, $\widetilde{E}_\mathrm{l}(r,z,\omega)$ is the Fourier transform of the electrical field of the driving laser $E_\mathrm{l}(r,z,t)$, and $\widetilde{G}_\mathrm{l}(r,z,\omega)$ accounts for the plasma effects. With Ω_p denoting the plasma frequency and the free electron density $n_\mathrm{e}(r,z,t)$ calculated from the Ammosov-Delone-Krainov model[16], $\widetilde{G}_\mathrm{l}$ is defined as

$$\widetilde{G}_\mathrm{l}(r,z,\omega) = \hat{F}\left[\frac{\Omega_\mathrm{p}^2(r,z,t)}{c^2} E_\mathrm{l}(r,z,t)\right], \quad (4)$$

$$\Omega_\mathrm{p}(r,z,t) = \sqrt{\frac{n_\mathrm{e}(r,z,t)}{m_\mathrm{e}\varepsilon_0}}, \quad (5)$$

where $\hat{F}$ represents the Fourier transform operator acting on the temporal coordinate, m_e is the electron mass, and ε_0 is the electronic permittivity. In Eq. (3), μ_0 is the permeability of vacuum, $\widetilde{E}_\mathrm{h}(r,z,\omega)$ is the Fourier transform of the electrical field of the harmonics $E_\mathrm{h}(r,z,t)$, and $\widetilde{P}_\mathrm{nl}(r,z,\omega)$ is the Fourier transform of the nonlinear polarization $P_\mathrm{nl}(r,z,t)$ generated by the gas. $P_\mathrm{nl}(r,z,t)$ is defined as

$$P_\mathrm{nl}(r,z,t) = (n_0 - n_\mathrm{e}) d_\mathrm{nl}(r,z,t), \quad (6)$$

where n_0 is the neutral atom density, and the nonlinear dipole moment $d_{\rm nl}(r,z,t)$ is calculated by the SFA model. Given that the harmonic frequencies are much larger than the plasma frequency, only the nonlinear dipole moment is considered in the source term on the right-hand side in Eq. (3). As a result, the plasma effects on the harmonic emission are introduced indirectly to the harmonic emission from the driving laser pulse. The onset of the ionization causes intensity and phase modulations to the driving laser field that greatly affect the phase and intensity of the source term in the right-hand of Eq. (3). This leads to the macroscopic phase matching effects for the harmonics. The low harmonic intensity in the 40–55 eV range is due to reabsorption of the gas medium.

The calculation parameters are the same as those used in the experiment for Fig. 1(b), except that the driving laser intensity is a little higher, which is still within the allowable error range. Figure 2(a) shows the full calculation result inclusive of the plasma effects under driving laser intensities 5×10^{14}, 7×10^{14}, 8×10^{14}, and 9×10^{14} W/cm^2. The four lines, plotted with different offsets vertically for clarity, correspond to the four driving laser intensities. The calculation concurs with the experiment. In Fig. 2(a), the harmonic emission is enhanced greatly as the driving laser intensity increases from 5×10^{14} to 7×10^{14} W/cm^2, and then it decays through intensities from 7×10^{14} to 9×10^{14} W/cm^2 . In contrast, no intensity decay is observed for the harmonic emission in Fig. 2(b) where the plasma effects are switched off. This indicates that the intensity-induced harmonic decay at high intensities is due to the plasma effects. Similarly, by comparing Figs. 2(a) and (b), the intensity-dependent spectral broadening and spectral blue shift observed in the experiment may also be due to the plasma effects. From Fig. 2(a), a phenomenon similar to the experimental result, which demonstrates the constant broadening of the harmonic spectrum towards the blue part as the driving laser intensity increases from 5×10^{14} to 9×10^{14} W/cm^2, is observed. When the ionization effects

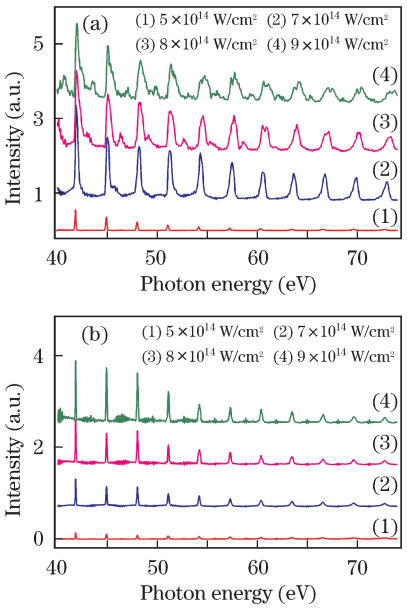

Fig. 2. Calculated harmonic spectra as a function of the driving laser intensity (a) with and (b) without plasma effects.

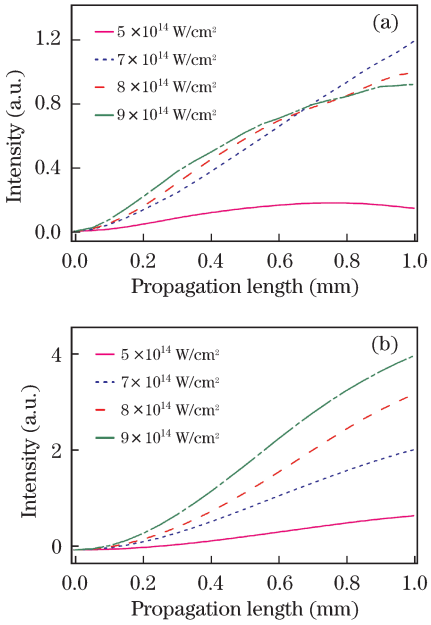

Fig. 3. Calculated intensity of the 41st harmonic as a function of the propagation length (a) with and (b) without plasma effects.

are switched off, the intensity-dependent spectral broadening and blue shift disappear, as shown in Fig. 2(b).

The harmonic signal was further analyzed as it accumulated through propagation to explore how the ionization-induced phase mismatch affected the aforementioned intensity-dependent feature. In Fig. 3, the 41st harmonic emission is calculated as a function of the propagation length with and without plasma. Compared with Fig. 3(b) where the effects of plasma on propagation are switched off, the harmonic emission in Fig. 3(a), with plasma effect included, is less efficient under all driving laser intensities. The ionization-induced driving laser diffraction leads to a decrease in driving laser intensity and, consequently, a decrease in the harmonic emission in the single atom response. As shown in Fig. 3, at a laser intensity of 5×10^{14} W/cm^2, the phase mismatch with plasma effects is larger than that without plasma effects. When the intensity increases to 7×10^{14} W/cm^2, the phase mismatch with plasma effects becomes smaller than that without plasma effects, which agrees with the conclusion for Fig. 1 that, at lower intensities, an increase in driving laser intensity leads to an increase in ionization, which improves the phase matching condition. Then, when the laser intensity increases from 7×10^{14} to 9×10^{14} W/cm^2, the phase mismatch with plasma effects becomes even larger than that without plasma effects. Therefore, the harmonic emission dependence on intensity may be attributed to the ionization effects in the phase matching process. This intensity-dependent change in the harmonic output energy is similar with that in Ref. [18]. Even though a supersonic gas jet with a much shorter interaction length was used in this letter instead of a long gas cell, the intensity dependence was still valid for the supersonic gas jet setup.

In conclusion, ionization effects on HHG have been investigated through macroscopic phase matching, both experimentally and theoretically, for a supersonic gas jet

source with short interaction length and high gas density. Comparison between the experimental results and numerical simulations under different considerations for ionization allows us to understand the role that ionization plays in the HHG process. Due to ionization, the harmonics show intensity-dependent features, such as harmonic conversion efficiency drop, spectral broadening, and spectral blue shift. These intensity-dependent phenomena are attributed to the ionization-induced propagation effects. Therefore, in a gas jet setup, an optimized harmonic output with tunable wavelength can be achieved by fine-tuning the driving laser intensity.

This work was supported by the Chinese Academy of Sciences, the Chinese Ministry of Science and Technology, the National Natural Science Foundation of China (Nos. 10734080, 10523003, 60921004, and 60978012), the National "973" Program of China (No. 2006CB806000), and the Shanghai Commission of Science and Technology (Nos. 06DZ22015 and 07pj14091).

References

1. H. C. Kapteyn, M. M. Murnane, and I. P. Christov, Physics Today **58,** (3) 39 (2005).
2. X. Zhu, B. Zhao, Y. Liu, Z. Miao, X. Zhang, and W. Zou, Acta Opt. Sin. (in Chinese) **28,** 1925, (2008).
3. Y. Zhang, D. Xing, and L. Liu, Chinese J. Lasers (in Chinese) **36,** 2609 (2009).
4. I. J. Kim, G. H. Lee, S. B. Park, Y. S. Lee, T. K. Kim, C. H. Nam, T. Mocek, and K. Jakubczak, Appl. Phys. Lett. **92,** 021125 (2008).
5. T. Popmintchev, M.-C. Chen, A. Bahabad, M. Gerrity, P. Sidorenko, O. Cohen, I. P. Christov, M. M. Murnane, and H. C. Kapteyn, PNAS **106,** 10516 (2009).
6. Y. Zheng, Z. Zeng, P. Zou, L. Zhang, X. Li, P. Liu, R. Li, and Z. Xu, Phys. Rev. Lett. **103,** 043904 (2009).
7. X. Chen, X. Li, J. Liu, P. Wei, X. Ge, R. Li, and Z. Xu, Opt. Lett. **32,** 2402 (2007).
8. Z. Zeng, Y. Cheng, X. Song, R. Li, and Z. Xu, Phys. Rev. Lett. **98,** 203901 (2007).
9. Y. Zheng, Z. Zeng, X. Li, X. Chen, P. Liu, H. Xiong, H. Lu, S. Zhao, P. Wei, L. Zhang, Z. Wang, J. Liu, Y. Cheng, R. Li, and Z. Xu, Opt. Lett. **33,** 234 (2008).
10. H. Xiong, R. Li, Z. Zeng, Y. Zheng, Y. Peng, X. Yang, X. Chen, H. Zeng, and Z. Xu, Phys. Rev. A **75,** 051802(R) (2007).
11. G. Chen, J. Chen, and Y. Yang, Acta Opt. Sin. (in Chinese) **29,** 3255 (2009).
12. R. Spitzenpfeil, S. Eyring, C. Kern, C. Ott, J. Lohbreier, J. Henneberger, N. Franke, S. Jung, D. Walter, M. Weger, C. Winterfeldt, T. Pfeifer, and C. Spielmann, Appl. Phys. A **96,** 69 (2009).
13. J. Itatani, J. Levesque, D. Zeidler, H. Niikura, H. Pépin, J. C. Kieffer, P. B. Corkum, and D. M. Villeneuve, Nature **432,** 867 (2004).
14. S. Baker, J. S. Robinson, C. A. Haworth, H. Teng, R. A. Smith, C. C. Chirilă, M. Lein, J. W. G. Tisch, and J. P. Marangos, Science **312,** 424 (2006).
15. C. Altucci, T. Starczewski, E. Mevel, C.-G. Wahlström, B. Caré, and A. L'Huillier, J. Opt. Soc. Am. B **13,** 148 (1996).
16. E. Priori, G. Cerullo, M. Nisoli, S. Stagira, S. De Silvestri, P. Villoresi, L. Poletto, P. Ceccherini, C. Altucci, R. Bruzzese, and C. de Lisio, Phys. Rev. A **61,** 063801 (2000).
17. M. Lewenstein, Ph. Balcou, M. Yu. Ivanov, A. L' Huillier, and P. B. Corkum, Phys. Rev. A **49,** 2117 (1994).
18. H. Dachraoui, T. Auguste, A. Helmstedt, P. Bartz, M. Michelswirth, N. Mueller, W. Pfeiffer, P. Salieres, and U. Heinzmann, J. Phys. B **42,** 175402 (2009).